Cite this article
Ahenkorah I, Rahman MM, Karim MR and Beecham S (2021)
Optimisation of chemical constituents on enzyme-induced carbonate precipitation in test-tube and soil. *Geotechnical Research* **8(3)**: 66–84,
https://doi.org/10.1680/jgere.21.00006

Research Article
Paper 2100006
Received 10/02/2021; Accepted 20/05/2021
Published online 21/06/2021
Published with permission by the ICE under the CC-BY 4.0 license.
(http://creativecommons.org/licenses/by/4.0/)

Keywords: calcium carbonate/cost/sustainability

Geotechnical Research

ice Publishing

Optimisation of chemical constituents on enzyme-induced carbonate precipitation in test-tube and soil

Isaac Ahenkorah BSc (Hons)
PhD candidate, SCaRCE, UniSA STEM, University of South Australia, Adelaide, Australia (Orcid:0000-0001-6044-1412)

Md Mizanur Rahman PhD, BSc (Hons)
Associate Professor in Geotechnical Engineering, SCaRCE, UniSA STEM, University of South Australia, Adelaide, Australia (Orcid:0000-0002-0638-4055) (corresponding author: Mizanur.Rahman@unisa.edu.au)

Md Rajibul Karim PhD, BSc (Hons)
Senior Lecturer, SCaRCE, UniSA STEM, University of South Australia, Adelaide, Australia (Orcid:0000-0002-5318-3862)

Simon Beecham PhD, BSc (Hons)
Professor, SCaRCE, UniSA STEM, University of South Australia, Adelaide, Australia (Orcid:0000-0002-9884-3852)

Enzyme-induced carbonate precipitation (EICP) is a bio-cementation technique and a sustainable method of ground improvement. This study examines the influence of the concentrations of substrates [S_0] and enzymes [E_0] as well as enzyme activity (A_E) on the calcium carbonate ($CaCO_3$) precipitation ratio (PR) using 130 test-tube experiments. It was found that the effect of enzyme concentration and activity on PR can be explained using a normalisation of [E_s] = [E_0] × A_E, where [E_s] is the adjusted enzyme concentration. PR increased non-linearly with increasing [E_s]/[S_0] and reached 100% at a threshold [E_s]/[S_0] value of approximately 20 kU/mol. An exponential function was developed that could capture the relationship between PR and [E_s]/[S_0] with reasonable accuracy. This observation was further evaluated with data from the literature consisting of a further 100 test-tube experiments. EICP solutions consisting of [E_s]/[S_0] = 20 kU/mol were found to be optimum for soil treatment. The established function was later extended to predict strength gain as measured by the unconfined compressive strength (UCS) and the splitting tensile strength (STS) for EICP-treated soils and could predict the strength gain (UCS/STS) with reasonable accuracy. Results from scanning electron microscopy images, energy-dispersive X-ray spectroscopy and X-ray powder diffraction showed that the precipitated calcium carbonate in test tubes and treated soil was mostly calcite crystals with different morphologies, possibly due to the level of purity of the urease enzyme used.

Notation

$[E_0]$	concentration of urease enzyme
$[E_s]$	normalised concentration of urease enzyme
e_0	initial void ratio of untreated Adelaide Industrial sand specimen
e_{AT}	void ratio after enzyme-induced carbonate precipitation soil treatment
D_r	initial relative density
d_{10}	soil particle size at 10% finer
d_{50}	soil particle size at 50% finer
e_{max}	maximum void ratio of soil
e_{min}	minimum void ratio of soil
M_{CaCO_3}	mass of precipitated calcium carbonate ($CaCO_3$)
N_{TC}	number of treatment cycles
q_t	splitting tensile strength
q_u	unconfined compressive strength
$[S_0]$	equimolar concentration of substrate (urea and calcium chloride ($CaCl_2$))

Introduction

Bio-cementation, notably microbially induced carbonate precipitation (MICP) and enzyme-induced carbonate precipitation (EICP), has been used to bind soil particles together through calcium carbonate ($CaCO_3$) precipitation in order to improve their strength and other mechanical properties (DeJong *et al.*, 2006; Hamdan and Kavazanjian, 2016; Ismail *et al.*, 2002; Mitchell and Santamarina, 2005). The precipitation of calcium carbonate in EICP occurs by way of a biogeochemical process – namely, urea hydrolysis catalysed by urease enzyme. Some MICP processes also use the same chemical pathway. Hydrolysis of urea ($CO(NH_2)_2$) into ammonium (NH_4^+) and carbonate ions (CO_3^{2-}) is the basis of calcium carbonate precipitation in the presence of divalent cations such as calcium (Ca^{2+}) ions, as presented in Equations I–V (Zimmer, 2000).

$$\text{I.}\quad CO(NH_2)_{2(s)} + H_2O_{(l)} \xrightarrow{\text{urease enzyme}} NH_{3(aq)} + CO(NH_2)OH_{(aq)}$$

$$\text{II.}\quad CO(NH_2)OH_{(aq)} + OH^-_{(aq)} \rightarrow NH_{3(aq)} + HCO_3^-(aq)$$

$$\text{III.}\quad NH_{3(aq)} + HCO_3^-(aq) \rightarrow NH_4^+(aq) + CO_3^{2-}(aq)$$

$$\text{IV.}\quad CaCl_{2(s)} \xrightarrow{H_2O} Ca^{2+}_{(aq)} + 2Cl^-_{(aq)}$$

$$\text{V.}\quad Ca^{2+}{}_{(aq)} + CO_3{}^{2-}(aq) \overset{\text{precipitation}}{\longleftrightarrow} CaCO_{3(s)}$$

MICP processes that involve urea hydrolysis require the growth of urease enzyme-producing aerobic bacteria that produce enzymes around their cells (DeJong *et al*., 2006; Rahman *et al*., 2020). However, the growth and culturing of bacteria can be a complex process since certain species of bacteria require particular growing conditions such as oxygen (O_2) availability, optimum pH and temperature (Almajed, 2017; Hamdan, 2015). The characteristics of these urease enzymes produced by bacterial cells are also not readily known and therefore the understanding of the influence of chemical constituents on calcium carbonate precipitation using catalytic reactions can be difficult (Nassar *et al*., 2018; Wen *et al*., 2020). On the other hand, EICP directly applies an enzyme that can be easily characterised before application (Ahenkorah *et al*., 2021). Potential applications of EICP include bio-cementation and bioremediation in many environmental, construction and engineering settings, such as improving soil strength, reducing soil liquefaction potential, surface erosion control, reducing permeability and heavy-metal contaminant remediation (Ahenkorah *et al*., 2020a; Hamdan, 2015; Krajewska, 2018; Neupane *et al*., 2015; Putra *et al*., 2017a).

Soil improvement through EICP treatment has been studied by several researchers. Yasuhara *et al*. (2012) achieved a maximum unconfined compressive strength (UCS) of 1.6 MPa for 300 g of Toyoura sand mixed with 0.50 M of urea–calcium chloride ($CaCl_2$) and 1.0 g of urease enzyme (with an activity of 2.95 kU/g). Almajed *et al*. (2018) also achieved a maximum UCS of 1.27 MPa for Ottawa 20-30 sand after four cycles of treatment using 1.0 M urea, 0.67 M calcium chloride and 3 g/l enzyme (with an activity of 3.50 kU/g). However, the cost of EICP treatment can be high. Commercially available pure urease enzyme is the most expensive component (~70–80% of the total cost) of the chemical constituents used. Some studies have utilised crude urease extract from different plant sources – for example, jack bean seeds/meal (Khodadadi *et al*., 2020; Nam *et al*., 2015), soybeans (Chen *et al*., 2021; Cuccurullo *et al*., 2019; Gao *et al*., 2019; Khodadadi *et al*., 2020; Lee and Kim, 2020; Pratama *et al*., 2021; Yuan *et al*., 2020) and watermelon seeds (Dilrukshi *et al*., 2018; Javadi *et al*., 2018; Khodadadi *et al*., 2020). Such plants can be a cost-effective source of enzyme and can be a viable pathway for large-scale application in the future. However, some extraction techniques may require additional processes or chemicals and may sometimes yield only a small quantity of urease enzymes (Khodadadi *et al*., 2020; Nam *et al*., 2015; Song *et al*., 2020).

The mechanism involved in urease enzymes catalysing the reaction and precipitation rate in EICP is not yet fully understood (Krajewska, 2009). It often shows a simple Michaelis–Menten behaviour (Michaelis and Menten, 1913). In a typical enzymatic reaction such as this, a substrate (e.g. urea) interacts with the enzyme and forms an enzyme–substrate complex, which is then converted to an enzyme–product complex. After formation of the product, the enzyme is freed up to form another enzyme–substrate complex. The rate of this reaction can be significantly dependent on the concentration and activity of the enzyme, as well as the availability of substrate to form the enzyme–substrate complex (Ahenkorah *et al*., 2021; Mazzei *et al*., 2014). The rate of reaction/precipitation can be further influenced by inhibitors such as a high urea concentration (Krajewska, 2009), a limited lifespan of free urease enzyme (Krajewska, 2018), pH and temperature (Ahenkorah *et al*., 2021).

Most studies on optimising the constituents in EICP treatment solutions have been conducted in test tubes at a standard initial pH and temperature of 8.0 and 25–30°C, respectively (Almajed *et al*., 2018; Hamdan, 2015; Neupane *et al*., 2013; Putra *et al*., 2015). These studies, summarised in Table 1, have generally used parametric approaches to evaluate the influence of the concentration of urea, calcium chloride, urease enzyme and enzyme activity (A_E) on the calcium carbonate precipitation ratio (PR – defined as the ratio of the mass of precipitated calcium carbonate to the theoretically possible maximum precipitation mass). Various concentrations have been proposed as being optimal in different studies along with some contradicting observations reported. For example, optimum ingredients for EICP treatment were an equimolar urea–calcium chloride concentration of 0.5 M with 2 g/l urease enzyme in the study by Neupane *et al*. (2013) and an equimolar concentration of 0.5 M urea–calcium chloride for 1 g/l urease enzyme in the study by Putra *et al*. (2015). Carmona *et al*. (2016) considered urease enzyme activity and treated an equimolar concentration of 0.25 M of urea–calcium chloride for 4 kU/l urease enzyme as optimum. Furthermore, Neupane *et al*. (2013) reported that for an equimolar concentration of urea–calcium chloride, PR increased rapidly with an

Table 1. Summary of previous studies on optimising the EICP process

Reference	$[E_0]$: g/l	A_E: kU/g	Urea: M	Calcium chloride: M	Curing time: days	Optimum chemical constituents		
						$[E_0]$: g/l	Calcium chloride: M	Urea: M
Neupane *et al*. (2013)	0.5–4.0	2.95	0.50–1.00	0.50–1.00	1	2.00	0.50	0.50
Hamdan (2015)	0.47	32.40	0.10–6.00	0.20–2.00	9	0.47	1.75/2	1.00
Putra *et al*. (2015)	1–5	2.95	0.50–1.50	0.50–1.50	1–7	1.00	0.50	0.50
Carmona *et al*. (2016)	4.0[a]	34.31	0.25–1.25	0.25–1.25	14	4.00[a]	0.25	0.25
Putra *et al*. (2017b)	1–2	2.95	0.50–1.00	0.50–1.00	3	2.00	0.50	0.50
Almajed *et al*. (2018)	1–6	3.50	0.25–1.50	0.14–1.50	3	3.00	0.67	1.00

[a] The concentration of enzyme used in this study was quantified in kilounits per litre

increase in urease enzyme concentration up to 3 g/l and the trend reversed afterwards. Putra *et al.* (2015) reported that PR increased with urease enzyme concentration and asymptoted at a maximum value of ~90%, with no reversal of the trend. Some studies using non-equimolar concentrations of urea–calcium chloride have also reported different concentrations of urea–calcium chloride as optimal. Hamdan (2015) reported an optimum urea–calcium chloride concentration ratio of 1.75:1 (M) for 0.47 g/l of urease enzyme. Almajed *et al.* (2018) found that a urea–calcium chloride concentration ratio of 1:0.67 (M) for 3 g/l urease enzyme was optimum.

In most previous studies, the influence of the urease enzyme activity has been overlooked or not captured appropriately. Furthermore, none of the previous studies has presented a simple framework that could be used to estimate the required quantities of enzyme and various chemicals for achieving a particular PR. Based on more than 100 test-tube experiments conducted, this study examines the interrelationships among concentrations of enzyme and different chemicals as well as enzyme activity and how they correlate with PR. A large data set from the literature was also compiled to validate the trend observed in this study.

The optimum concentration of chemical constituents established in this study was used for soil treatment. The treated samples were tested for UCS, splitting tensile strength (STS) and the mass of precipitated calcium carbonate (M_{CaCO_3}). A model was developed that could predict the amount of precipitated calcium carbonate and strength (UCS/STS) of a particular soil with known concentrations of chemicals used in the treatment process. Scanning electron microscopy (SEM) imaging, energy-dispersive X-ray spectroscopy (EDS) analysis and X-ray powder diffraction (XRD) analysis were used to evaluate the microstructure of the precipitated calcium carbonate in test tubes and in treated soil.

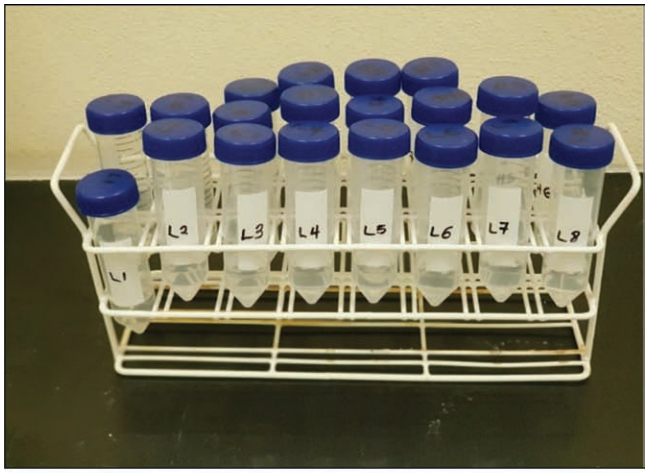

(a)

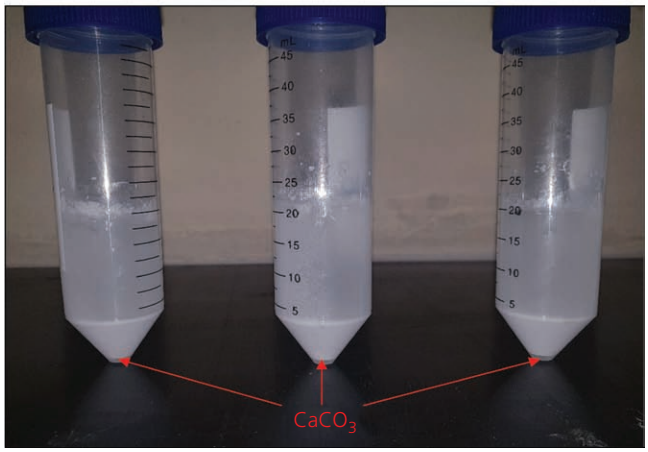

(b)

Figure 1. (a) Test tubes with EICP solution during the curing stage; (b) precipitated calcium carbonate in test tubes after curing (for 10 days)

Laboratory investigation

Test-tube experiments

As part of this study, a total of 130 precipitation tests were carried out using 50 ml test tubes containing 20 ml of EICP solution consisting of a mixture of urea, calcium chloride and enzyme (Figure 1(a)). To evaluate the influence of urease enzyme activity – that is, A_E – two different types of urease enzyme – namely, high-activity enzyme (HAE) with A_E = 40.15 kU/g and low-activity enzyme (LAE) with A_E = 3.50 kU/g extracted from jack beans, supplied by Sigma-Aldrich and Fisher Scientific, respectively – were used. The enzyme concentration, $[E_0]$, was varied between 0 and 20 kU/l (corresponding to 0–0.42 g/l for HAE and 0–5.10 g/l for LAE). These ranges of $[E_0]$ were selected based on the ranges of concentrations used in previous studies (Almajed *et al.*, 2018; Neupane *et al.*, 2013; Putra *et al.*, 2015). An equimolar concentration $[S_0]$ of 0–1.3 M for urea–calcium chloride was used in this study after the thesis by Hamdan (2015), who reported that an equimolar ratio of urea–calcium chloride may produce an equal proportion of carbonate and calcium ions required for the production of calcium carbonate, and these ions may become limited if non-equimolar ratios are used. Details of all the tests are presented in Tables 2 and 3.

An initial curing period of 10 days was used for all tests based on existing knowledge from the literature (Almajed *et al.*, 2018; Hamdan, 2015; Neupane *et al.*, 2013; Putra *et al.*, 2015). Besides, the rate of calcium carbonate precipitation was assessed over a curing period of 10 days (i.e. at 12, 24, 36, 48 and 72 h and continued for 10 days) using the optimum concentration of chemical constituents established in this study. After curing, the solution in each test tube (Figure 1(b)) was filtered using ashless filter papers (11 µm) and then oven-dried at 60°C. Afterwards, the masses of the dried precipitates remaining on the filter paper and in the test tube were measured and the total precipitated mass was obtained. PR (%) was calculated as the ratio of precipitated total calcium carbonate to theoretical maximum precipitation mass. The theoretical precipitation mass of calcium carbonate (g) was

Table 2. Summary of calcium carbonate precipitation in test tubes for HAE (A_E = 40.15 kU/g)

Test	Urea–calcium chloride, $[S_0]$: M	Enzyme, $[E_0]$: g/l	Enzyme, $[E_s] = [E_0] \times A_E$: kU/l	Theoretical mass: g	Precipitated mass: g	PR: %
H1	0.05	0.123	4.95	0.100	0.099	99
H2	0.10	0.111	4.45	0.200	0.199	99
H3	0.10	0.323	12.95	0.200	0.200	100
H4	0.10	0.401	16.10	0.200	0.200	100
H5	0.10	0.418	16.80	0.200	0.200	100
H6	0.15	0.105	4.20	0.300	0.288	96
H7	0.20	0.086	3.45	0.400	0.383	96
H8	0.20	0.288	11.55	0.400	0.399	100
H9	0.20	0.366	14.70	0.400	0.400	100
H10	0.20	0.384	15.40	0.400	0.400	100
H11	0.25	0.073	2.95	0.500	0.427	85
H12	0.30	0.061	2.45	0.601	0.448	75
H13	0.30	0.253	10.15	0.601	0.592	99
H14	0.30	0.331	13.30	0.601	0.595	99
H15	0.30	0.349	14.00	0.601	0.592	99
H16	0.35	0.049	1.95	0.701	0.468	67
H17	0.35	0.055	2.20	0.701	0.492	70
H18	0.40	0.036	1.45	0.801	0.412	51
H19	0.40	0.218	8.75	0.801	0.782	98
H20	0.40	0.296	11.90	0.801	0.784	98
H21	0.40	0.314	12.60	0.801	0.793	99
H22	0.45	0.024	0.95	0.901	0.332	37
H23	0.50	0.017	0.70	1.001	0.285	28
H24	0.50	0.183	7.35	1.001	0.946	95
H25	0.50	0.200	8.05	1.001	0.959	96
H26	0.50	0.262	10.50	1.001	0.977	98
H27	0.50	0.279	11.20	1.001	0.979	98
H28	0.55	0.000	0.00	1.101	0.000	0
H29	0.55	0.005	0.20	1.101	0.115	10
H30	0.60	0.148	5.95	1.201	0.925	77
H31	0.60	0.227	9.10	1.201	1.136	95
H32	0.60	0.244	9.80	1.201	1.152	96
H33	0.70	0.113	4.55	1.401	0.927	66
H34	0.70	0.131	5.25	1.401	1.014	72
H35	0.70	0.192	7.70	1.401	1.260	90
H36	0.70	0.209	8.40	1.401	1.262	90
H37	0.80	0.078	3.15	1.601	0.735	46
H38	0.80	0.096	3.85	1.601	0.851	53
H39	0.80	0.157	6.30	1.601	1.171	73
H40	0.80	0.174	7.00	1.601	1.405	88
H41	0.90	0.044	1.75	1.802	0.638	35
H42	0.90	0.061	2.45	1.802	0.614	34
H43	0.90	0.122	4.90	1.802	1.141	63
H44	0.90	0.139	5.60	1.802	1.294	72
H45	1.00	0.009	0.35	2.002	0.132	7
H46	1.00	0.026	1.05	2.002	0.479	24
H47	1.00	0.087	3.50	2.002	0.956	48
H48	1.00	0.105	4.20	2.002	1.005	50
H49	1.10	0.000	0.00	2.202	0.000	0
H50	1.10	0.052	2.10	2.202	0.779	35
H51	1.10	0.070	2.80	2.202	0.888	40
H52	1.20	0.017	0.70	2.402	0.307	13
H53	1.20	0.035	1.40	2.402	0.520	22
H54	1.30	0.000	0.00	2.602	0.000	0

evaluated as $C \times V \times M$, where C and V represent the substrate concentration in moles per litre and the volume of the EICP solution in litres, respectively, and M is the molar mass of calcium carbonate (i.e. 100.087 g/mol).

Treatment of soil using EICP and strength tests

Soil sample preparation

A commercially available sand – namely, Adelaide Industrial (AI) sand (e_{min} = 0.68 and e_{max} = 1.05) – was used in the current study.

Table 3. Summary of calcium carbonate precipitation in test tubes for LAE (A_E = 3.50 kU/g)

Test	Urea–calcium chloride, $[S_0]$: M	Enzyme, $[E_0]$: g/l	Enzyme, $[E_s] = [E_0] \times A_E$: kU/l	Theoretical mass: g	Precipitated mass: g	PR: %
L1	0.10	1.200	4.20	0.200	0.197	98
L2	0.10	4.600	16.10	0.200	0.199	99
L3	0.10	4.800	16.80	0.200	0.200	100
L4	0.20	1.100	3.85	0.400	0.391	98
L5	0.20	4.200	14.70	0.400	0.398	99
L6	0.20	4.400	15.40	0.400	0.399	100
L7	0.30	0.900	3.15	0.601	0.575	96
L8	0.30	1.000	3.50	0.601	0.585	97
L9	0.30	3.800	13.30	0.601	0.591	98
L10	0.30	4.000	14.00	0.601	0.593	99
L11	0.40	0.800	2.80	0.801	0.776	97
L12	0.40	3.400	11.90	0.801	0.789	99
L13	0.40	3.600	12.60	0.801	0.790	99
L14	0.50	0.600	2.10	1.001	0.819	82
L15	0.50	0.700	2.45	1.001	0.893	89
L16	0.50	3.000	10.50	1.001	0.985	98
L17	0.50	3.200	11.20	1.001	0.988	99
L18	0.50	4.800	16.80	1.001	0.993	99
L19	0.50	5.100	17.85	1.001	0.991	99
L20	0.60	0.400	1.40	1.201	0.742	62
L21	0.60	0.500	1.75	1.201	0.810	67
L22	0.60	2.600	9.10	1.201	1.130	94
L23	0.60	2.800	9.80	1.201	1.158	96
L24	0.60	4.200	14.70	1.201	1.199	100
L25	0.60	4.500	15.75	1.201	1.195	99
L26	0.70	0.200	0.70	1.401	0.433	31
L27	0.70	0.300	1.05	1.401	0.614	44
L28	0.70	2.200	7.70	1.401	1.270	91
L29	0.70	2.400	8.40	1.401	1.290	92
L30	0.70	3.600	12.60	1.401	1.351	96
L31	0.70	3.900	13.65	1.401	1.368	98
L32	0.80	0.000	0.00	1.601	0.000	0
L33	0.80	0.100	0.35	1.601	0.270	17
L34	0.80	1.800	6.30	1.601	1.300	81
L35	0.80	2.000	7.00	1.601	1.360	85
L36	0.90	3.000	10.50	1.802	1.626	90
L37	0.90	3.300	11.55	1.802	1.705	95
L38	0.90	1.400	4.90	1.802	1.200	67
L39	0.90	1.600	5.60	1.802	1.340	74
L40	1.00	1.000	3.50	2.002	1.080	54
L41	1.00	1.200	4.20	2.002	1.180	59
L42	1.10	0.600	2.10	2.202	0.740	34
L43	1.10	0.800	2.80	2.202	0.910	41
L44	1.10	2.400	8.40	2.202	1.829	83
L45	1.10	2.700	9.45	2.202	1.914	87
L46	1.20	0.200	0.70	2.402	0.280	12
L47	1.20	0.400	1.40	2.402	0.530	22
L48	1.20	1.800	6.30	2.402	1.596	66
L49	1.20	2.100	7.35	2.402	1.737	72
L50	1.30	0.000	0.00	2.602	0.000	0
L51	1.30	1.200	4.20	2.602	1.319	51
L52	1.30	1.500	5.25	2.602	1.483	57

Figures 2(a) and 2(b) show the particle size distribution and one batch of treated specimen, respectively. AI sand particles are poorly graded according to the Unified Soil Classification System (ASTM, 2017a), being angular to subangular in shape. The samples were prepared in a cylindrical poly(vinyl chloride) (PVC) split mould (50 mm diameter × 100 mm height). An initial moisture content of 10% (Figure 3(a)) and void ratio, e_0, of 0.93 (D_r = 33%) were maintained during the placement of sand in the mould. Scouring pad filters were placed on both the top and bottom of the mould to minimise possible losses of soil particles during treatment.

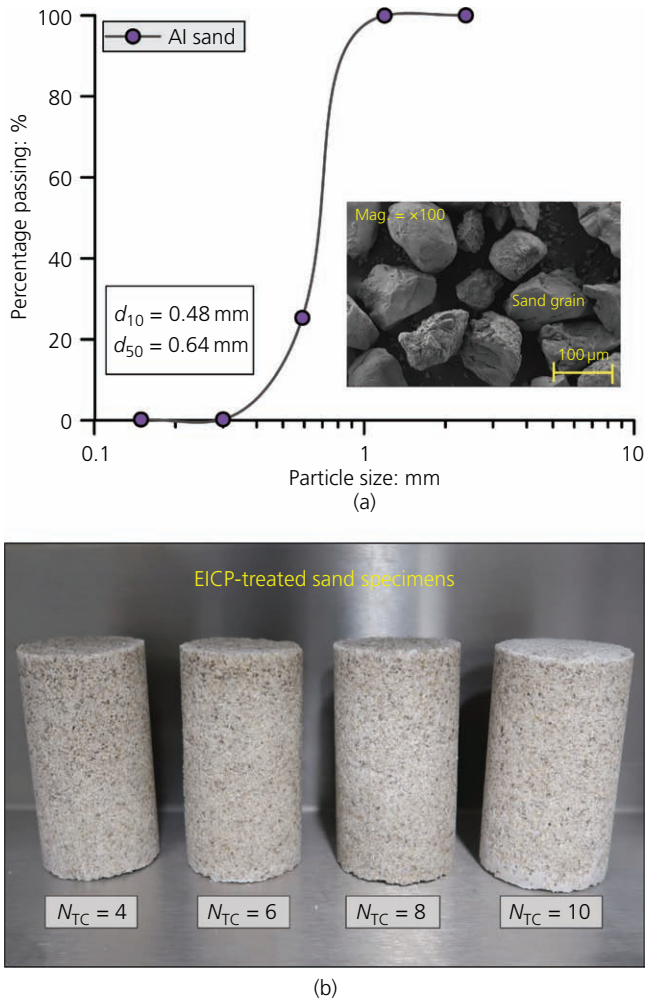

Figure 2. (a) Particle size distribution curve of Al sand; (b) image of EICP-treated sand specimens

EICP soil treatment

For EICP soil treatment, a similar approach as described previously by Ahenkorah *et al*. (2020a) was adopted. The EICP treatment solution consisted of a mixture of enzyme solution (ES) and cementation solution (CS). The ES was prepared by mixing the enzyme powder (LAE or HAE) and a stabiliser (4.0 g/l of non-fat dry milk powder) with deionised water and then filtered using 11 µm filter paper to remove undissolved impurities (Ahenkorah *et al*., 2020a). Based on the observations from the test-tube experiments, an optimum $[E_s]/[S_0]$ of 20 kU/mol was used for the soil treatment. This corresponds to an enzyme concentration $[E_s]$ of ~10 kU/l (i.e. 0.25 g/l and 3 g/l for HAE and LAE, respectively) and CS – that is, $[S_0]$ – of 0.50 M (equimolar) for urea–calcium chloride. Note, $[E_s] = [E_0] \times A_E$, where $[E_s]$ is the adjusted enzyme concentration.

To produce various levels of cementation for different samples, four, six, eight and ten treatment cycles (N_{TC}) were used. Each EICP treatment cycle consisted of one injection of 80 ml (~1 pore volume) of EICP treatment solution (i.e. a mixture of ES and CS) into the sand column by way of gravity percolation from the top (Figure 3((b)). The injection period for each sample lasted for approximately 5 min. The top and bottom valves of the mould were then closed to prevent solution losses, and the sample was cured at 30°C for ~2–3 days after each treatment cycle (Figure 3(c)). Therefore, a specimen with ten treatment cycles had a total treatment duration of 3–4 weeks. The curing time was selected based on observations from the test-tube experiments. The flow direction was reversed by flipping the samples upside down in every alternate cycle to promote more homogeneous precipitation (Ahenkorah *et al*., 2020a; Martinez *et al*., 2013; Nafisi *et al*., 2019). After curing in each cycle, the sample was drained under gravity by way of the base outlet (Figures 3(d) and 3(e)) before the next treatment cycle was applied. After the final treatment cycle, the treated specimens were oven-dried at 60°C for 48 h (Ahenkorah *et al*., 2020a; Whiffin, 2004) until a constant mass was achieved, and the sample was then stored for UCS/STS testing (Figure 3(f)).

Mechanical behaviour testing

A total of 16 EICP-treated specimens (using LAE or HAE) were prepared for UCS (ASTM, 2016) and STS (ASTM, 2017b) testing under a constant rate of deformation of 1.0 mm/min. The strain in the UCS test was calculated by dividing the deformation by the initial length of the sample, and the strain in the STS tests was calculated as the ratio of the diametrical displacement to specimen diameter (ASTM, 2017b). The stress in the STS tests was calculated as $\sigma_T = 2P/\pi LD$, where σ_T is the splitting tensile stress; P is the splitting tensile load; and L and D are the length and diameter of the specimen, respectively.

Measurements of calcium carbonate content

After completion of the UCS and STS tests, each sample was divided into six segments. The mass of precipitated calcium carbonate (M_{CaCO_3}) in each segment was determined using a gravimetric acid washing technique (Choi *et al*., 2017; Mortensen and DeJong, 2011). This involved the soaking of each specimen segment in 1 M hydrochloric acid (HCl) until it stopped seething. All samples were flushed with tap water before and after the acid washing to remove any residual chemical reagents. The difference in mass of the specimen before and after acid digestion was recorded as the net M_{CaCO_3} within the soil (Mahawish *et al*., 2019; Mortensen and DeJong, 2011; Xiao *et al*., 2019).

Microstructural analysis of the precipitated calcium carbonate

The influence of urease enzyme activity (HAE and LAE) on the microstructure of the precipitated calcium carbonate in both test tubes and in EICP-treated soil was evaluated using SEM, EDS and XRD analysis. For the SEM and EDS analyses, oven-dried calcium carbonate precipitates from the test-tube experiments and 25 mm cylindrical polished blocks prepared from the untreated and EICP-treated Al sand specimens were used. Each sample was

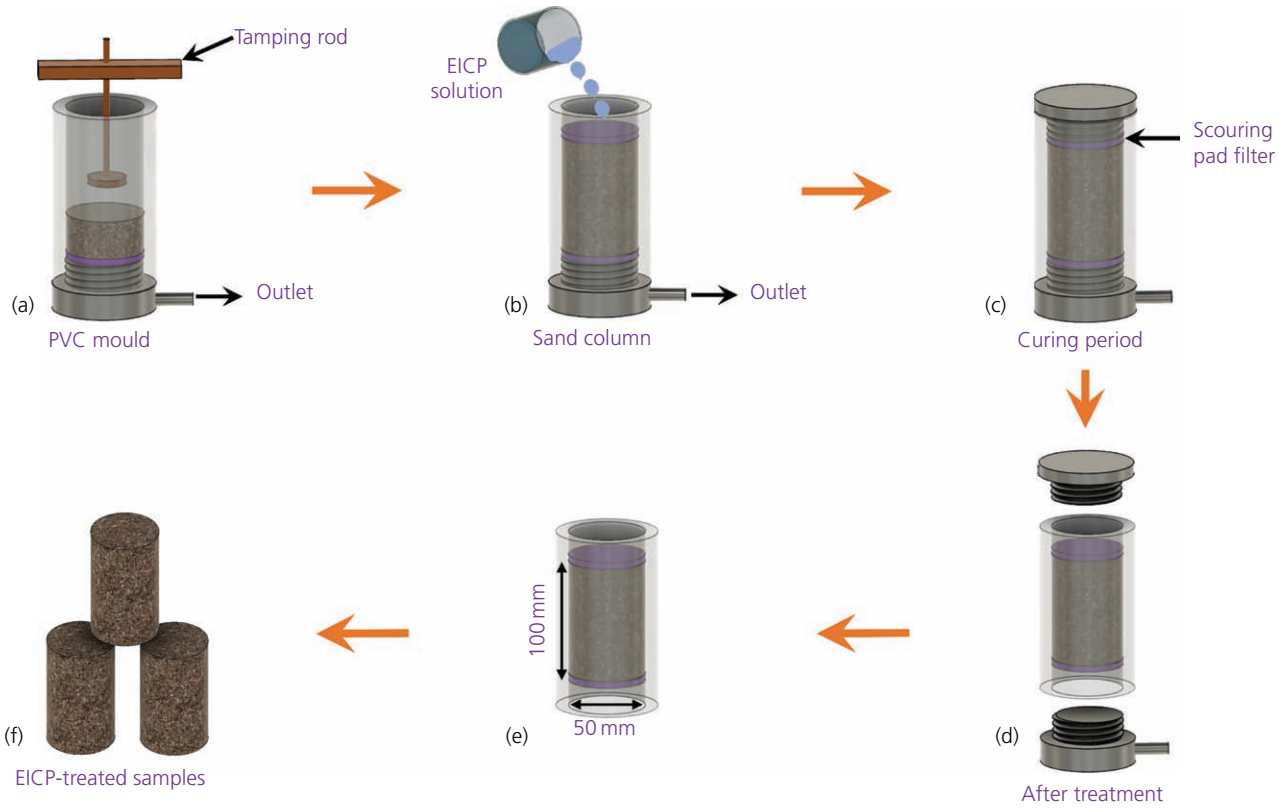

Figure 3. EICP treatment method: (a) preparation of untreated sand columns; (b) injecting EICP solution into the sand column; (c) treatment (curing) of sand columns; (d) drainage of sand columns after treatment period; (e) separation of specimen and PVC mould; (f) EICP-treated samples

sputter-coated using a high-resolution carbon (C) sputter coater before SEM and EDS were carried out by using a high-resolution Carl Zeiss Merlin field emission gun scanning electron microscope.

For XRD analysis, samples were ground using a sterile mortar and pestle before performing XRD (Panalytical Empyrean). The angle of diffraction (2θ) of the X-rays was set from 10 to 80°, with a step size of 0.02°, and the scanning speed was set at 4°/min using copper (Cu) Kα.

Results

Effect of constituent concentrations on test-tube calcium carbonate precipitation

In Figure 4(a), PR is plotted against the equimolar concentration [S_0] of urea–calcium chloride for a selected range of different enzyme concentrations [E_0]. For all enzyme concentrations (both HAE and LAE), PR decreased with an increase in [S_0]. This was probably due to the enzyme concentration and activity not being high enough to convert all substrates into products within the designated curing period, particularly for high [S_0]. Figure 4(b) plots PR against [E_0] (g/l) for four different substrate concentrations (0.1–1.0 M). For all [S_0], PR increased with an increase in [E_0]. However, HAE and LAE exhibited different rates of gain for PR against [E_0]. The data from Figure 4(b) are replotted in Figure 4(c), but this time, the enzyme concentration is adjusted for its activity (i.e. [E_s] in kU/l = [E_0] in g/l × A_E in kU/g). The differences in the rate of gain of PR for HAE and LAE reduce significantly. It appears that a simple assumption of a normalised enzyme concentration by accounting for its activity works reasonably well in explaining the changes in PR for different enzyme activities. In Figures 4(b) and 4(c), a threshold is observed beyond which the effect of an increase in urease enzyme concentration is negligible.

Figure 5(a) shows the PR from all the tests conducted in this study plotted against [E_0] and [S_0] in a three-dimensional plot. This shows that the PR values from tests using LAE and HAE fall on two distinct surfaces (indicated as surfaces 1 and 2), and when [E_0] was adjusted for its activity (see Figure 5(b)), the two surfaces merged (indicated as surface 3). To evaluate further the existence of the trend observed in Figure 5(b), more than 100 data points for similar test-tube studies were collected from the literature (Almajed *et al.*, 2018; Carmona *et al.*, 2016; Hamdan, 2015; Neupane *et al.*, 2013; Putra *et al.*, 2015). Standard initial pH and temperature values of 7.0–8.0 and 25–30°C, respectively, were maintained in selecting the data sets. The curing period of

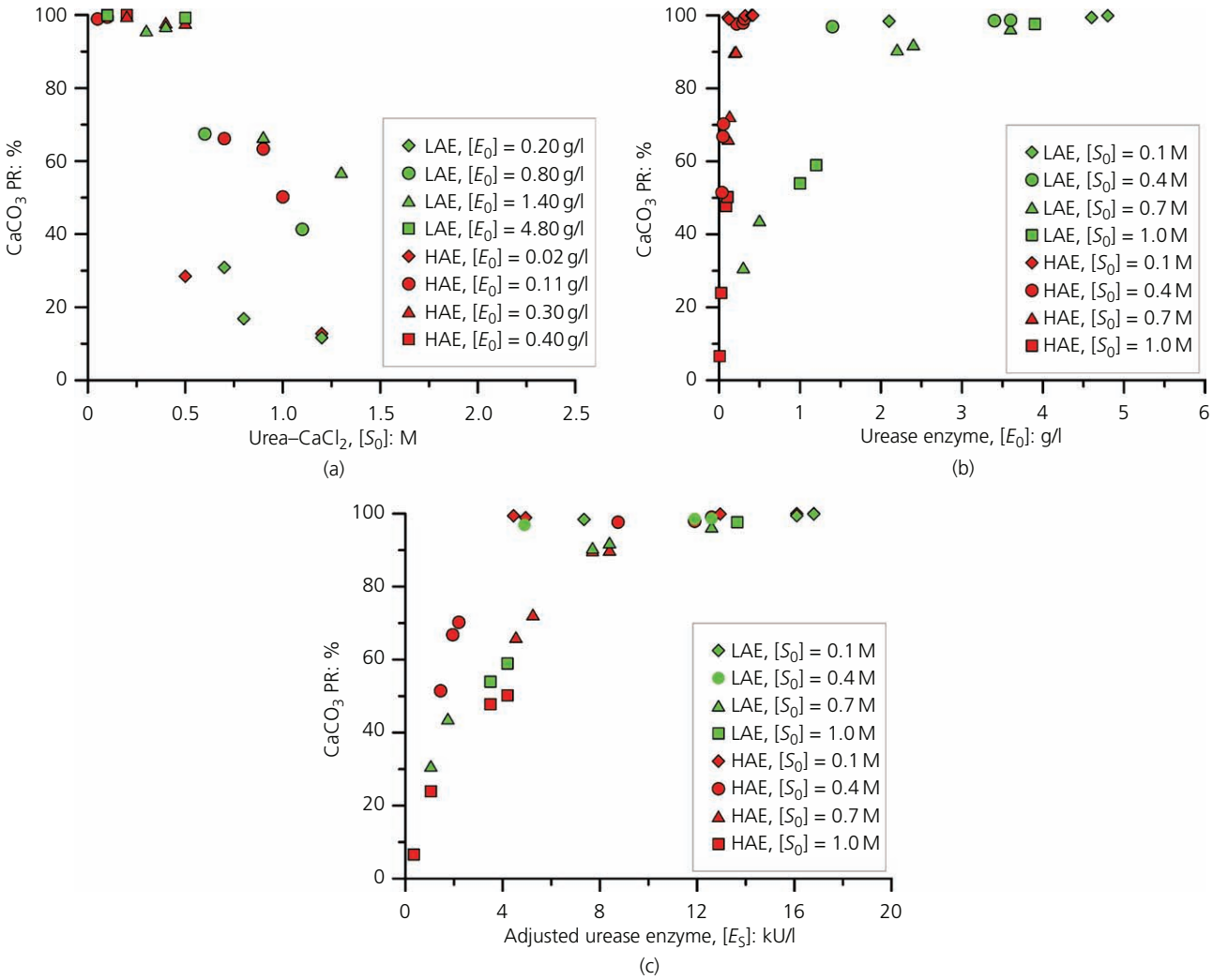

Figure 4. PR plotted against (a) urea–calcium chloride concentration, $[S_0]$; (b) enzyme concentration, $[E_0]$ (g/l); and (c) $[E_s]$ adjusted for activity (kU/l)

these data varied from 1 to 14 days. These data are presented in Figure 5(c), and despite having variations in curing period, they follow a similar trend as observed in Figure 5(b).

Three-dimensional non-linear regression analyses were performed using the Matlab R2020a software to determine the best-fit surface function for the observed trend in Figures 5(b) and 5(c). The best three surface functions were chosen, and their relative performances were compared using the root mean square deviation (RMSD), the sum of squares error (SSE) and the coefficient of determination (R^2) as presented in Table 4. It was observed that the exponential surface function (ESF) produced a good correlation with the maximum R^2 and minimum RMSD and SSE (Table 4). The surface function is presented in Figures 5(b) and 5(c), which gave an R^2 of 0.989 and 0.957 for data from this study and data from the literature, respectively.

To understand better the attributes of the ESF presented in Table 4, the data points in Figures 5(b) and 5(c) were plotted in PR against $[E_s]/[S_0]$ space, and these are shown in Figures 6(a) and 6(b), respectively. All the data fall on a line traced by the ESF in Table 4. It is interesting to note from Figures 6(a) and 6(b) that PR increases with an increase in $[E_s]/[S_0]$ up to a threshold value of approximately 20 kU/mol and asymptotes at PR = 100% after that.

As shown in Figure 7, for the same $[E_s]/[S_0]$ of 20 kU/mol, the PR for both HAE and LAE increased steadily with time at the beginning of the test. The maximum PR was obtained after ~3 days of curing (reaction) time and remained approximately constant until the end of the curing period (10 days). It is worth noting that for a particular $[E_s]/[S_0]$, the trend achieved in Figure 7 could be different due to the degradation of urease enzyme over time and/or product inhibition.

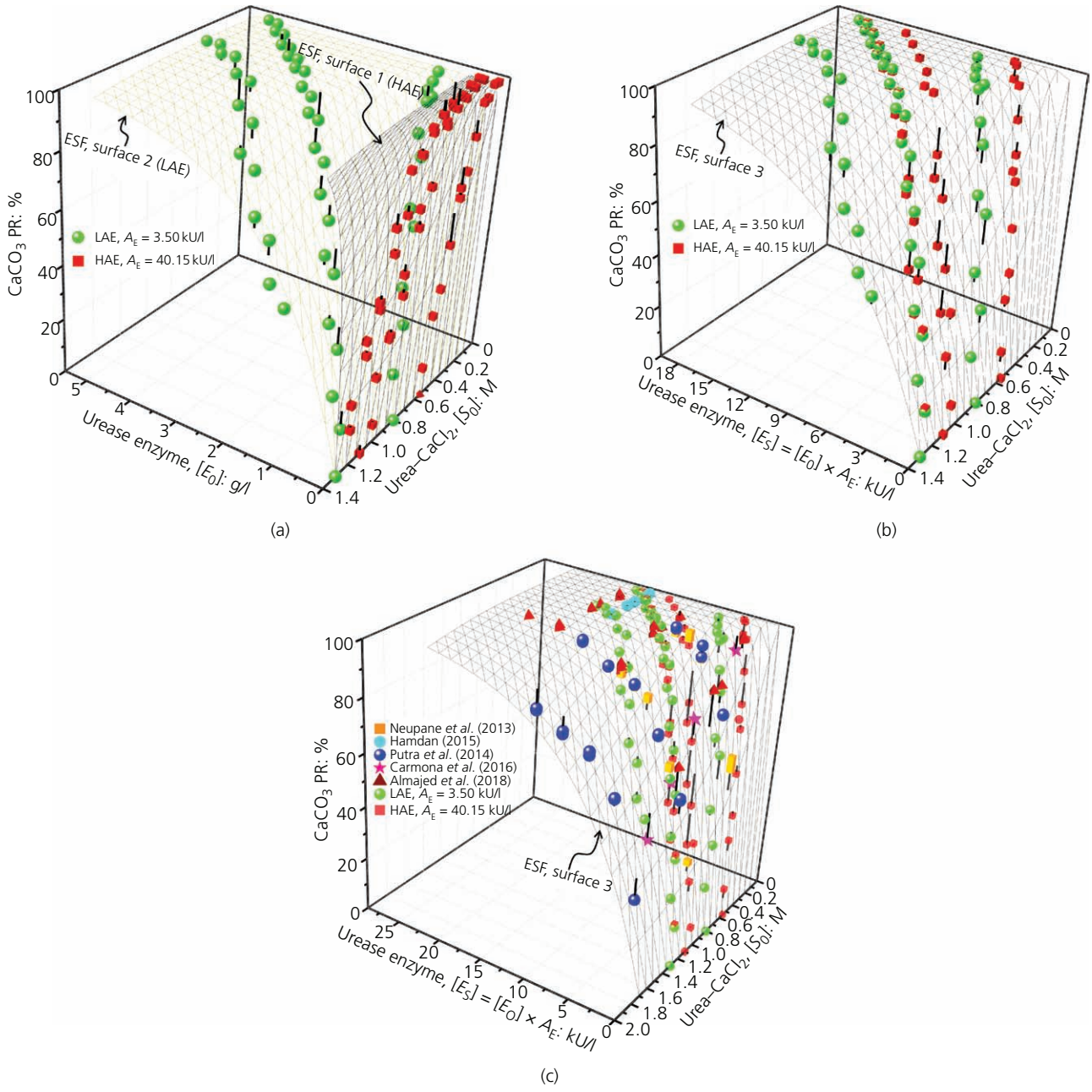

Figure 5. Three-dimensional plot of PR, $[E_s]$ and $[S_0]$ with the exponential surface function as a mesh for (a) enzyme concentration, $[E_0]$ (g/l); (b) $[E_s]$ adjusted for activity (kU/l); and (c) both data from this study and data from previous studies

Evaluation of EICP-treated AI sands

Precipitated calcium carbonate within EICP-treated sand

An expression for estimating M_{CaCO_3} can be developed from the ESF equation presented in Table 4 as follows:

1. $$CaCO_3(g) = [1 - \exp(-0.2035 \times [E_s]/[S_0])] \times M_t$$

where M_t is the maximum theoretical mass of precipitated calcium carbonate for a given substrate concentration. Figure 8 shows the relationship between the laboratory-measured M_{CaCO_3} (using the acid washing technique) and the model-predicted M_{CaCO_3} (using Equation 1) for UCS and STS samples in this study and data from previous studies. An excellent agreement was achieved with an R^2 of 0.984. Also to be noted is that when $[E_s]/[S_0]$ is plotted against the PR for treated samples, they fall on a line traced by the ESF.

Table 4. Performance comparison of different surface functions

Name	Equation	This study			Data from the literature		
		RMSD	SSE	R^2	RMSD	SSE	R^2
ESF	$PR(\%) = 100 \times [1 - \exp(-0.2035 \times [E_s]/[S_0])]$	3.374	1195	0.989	4.046	10 730	0.957
PSF	$PR(\%) = 73.7 + (15.4 \times [E_s]) - (124.0 \times [S_0]) - (0.6 \times [E_s]^2)(51.9 \times [S_0]^2)$ $0 \le PR \le 100$, $[E_s] > 0$ and $[S_0] > 0$	4.315	1955	0.982	10.730	11 600	0.711
RSF	$PR(\%) = [100 \times ([E_s]/[S_0])]/[3.5 + ([E_s]/[S_0])]$	8.783	8178	0.969	12.304	13 517	0.903

ESF, exponential surface function; PSF, polynomial surface function; RSF, rational surface function

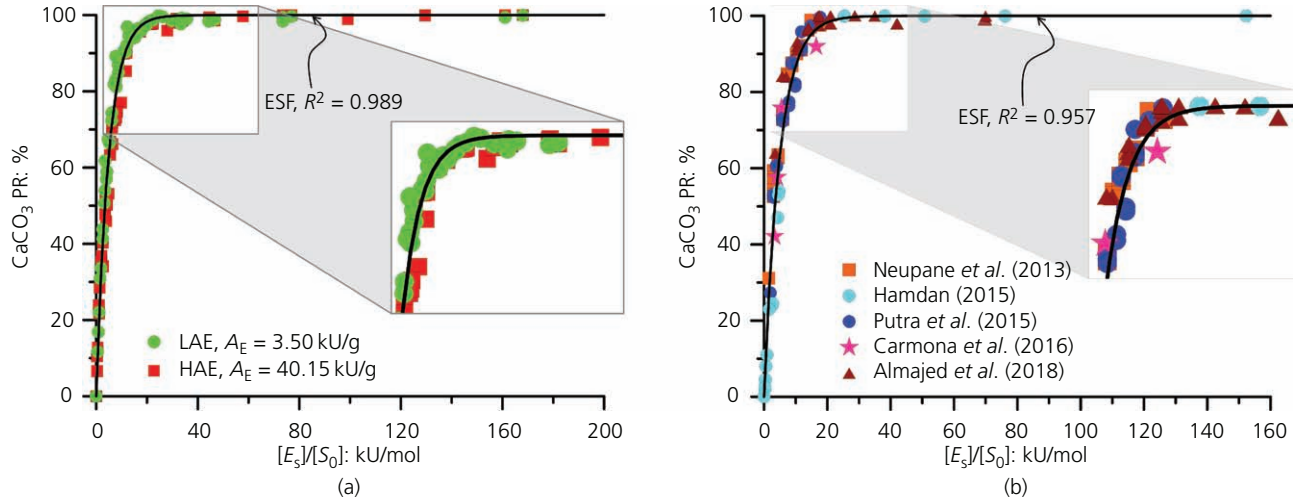

Figure 6. Plot of PR against $[E_s]/[S_0]$ for (a) test-tube experimental data using HAE and LAE and (b) data from previous studies

Stress–strain behaviour for UCS and STS

The UCS and STS test results are summarised in Table 5. Typical stress-against-strain curves for different N_{TC} are shown in Figures 9(a) and 9(b) for the UCS tests and in Figures 9(c) and 9(d) for the STS tests. For EICP treatments using an optimum $[E_s]/[S_0]$ of 20 kU/mol, both UCS and strain at failure increase with an increasing N_{TC} and similar strengths for the treated samples were achieved with a similar number of treatments. For example, samples treated with HAE had UCS values of 0.48 and 2.82 MPa for N_{TC} of 4 and 10, respectively (Figure 9(a)). Corresponding samples treated with LAE

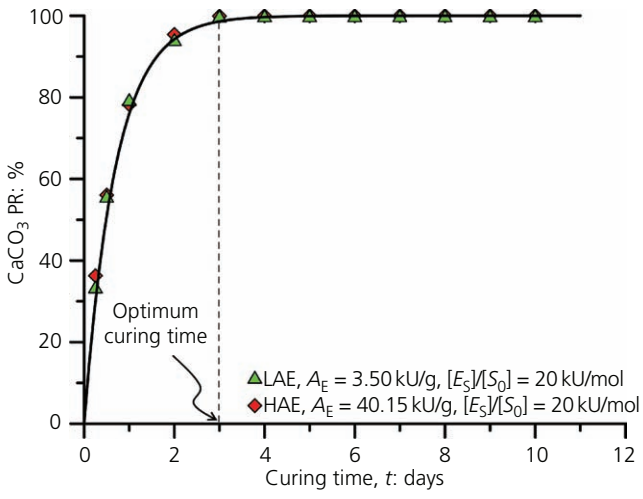

Figure 7. Plot of PR against reaction/curing time

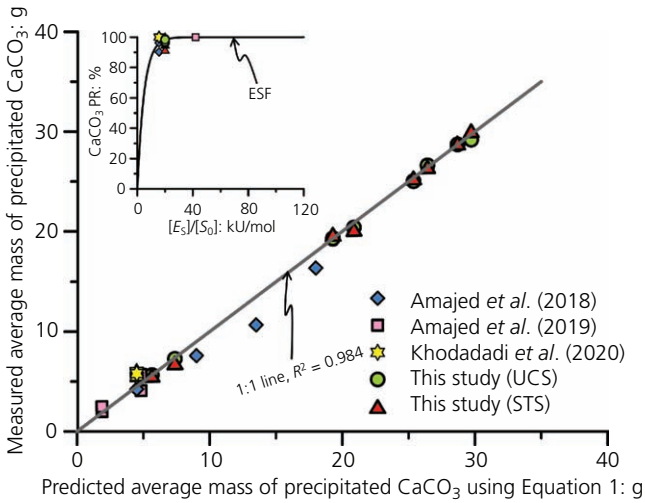

Figure 8. Relationship between model-predicted (using Equation 1) and measured average precipitated calcium carbonate for UCS and STS specimens, compared with data from previous studies

Table 5. Results of UCS and STS tests for AI sand

ID	Type of enzyme	Test	N_{TC}	After treatment void ratio, e_{AT}	Strength: MPa	$[E_s]/[S_0]$: kU/mol	M_t: g	M_{CaCO_3}: g	PR: %
H1	HAE	UCS	4	0.870	0.482	20	7.50	7.28	97
L1	LAE	UCS	4	0.880	0.432	20	5.74	5.65	96
H2	HAE	UCS	6	0.787	1.344	20	21.24	20.39	99
L2	LAE	UCS	6	0.798	1.164	20	19.63	19.31	97
H3	HAE	UCS	8	0.758	1.961	20	26.88	26.61	98
L3	LAE	UCS	8	0.766	1.823	20	25.81	25.04	98
H4	HAE	UCS	10	0.744	2.819	20	30.24	29.19	97
L4	LAE	UCS	10	0.746	2.713	20	29.19	28.72	98
H5	HAE	STS	4	0.872	0.167	20	7.50	6.88	92
L5	LAE	STS	4	0.880	0.161	20	5.74	5.62	98
H6	HAE	STS	6	0.793	0.272	20	21.24	20.20	95
L6	LAE	STS	6	0.796	0.268	20	19.63	19.70	100
H7	HAE	STS	8	0.758	0.447	20	26.88	26.48	99
L7	LAE	STS	8	0.765	0.421	20	25.81	25.35	98
H8	HAE	STS	10	0.739	0.628	20	30.24	30.08	99
L8	LAE	STS	10	0.746	0.573	20	29.19	28.85	99

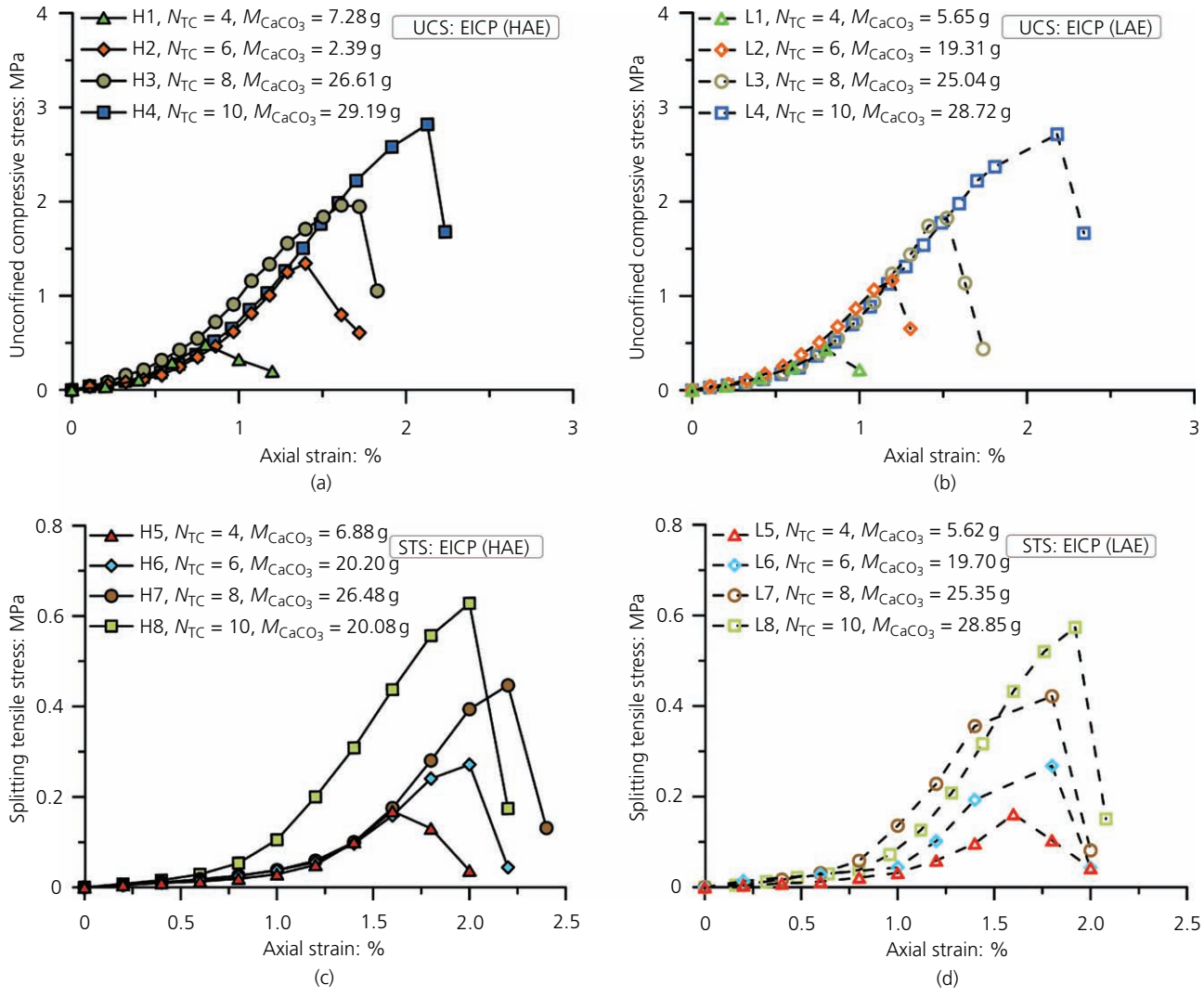

Figure 9. Unconfined compressive stress–strain behaviour of EICP-treated sand for different N_{TC} values using (a) HAE and (b) LAE; splitting tensile stress–strain behaviour of EICP-treated sand for different N_{TC} values using (c) HAE and (d) LAE

achieved UCS values of 0.43 and 2.71 MPa for N_{TC} of 4 and 10, respectively (Figure 9(b)).

Figures 9(c) and 9(d) show the splitting tensile stress–strain behaviour of EICP-treated AI sand using HAE and LAE. Similar to the observed UCS test behaviour, STS increases with increasing N_{TC} and the strength gains were similar. For specimens treated with HAE, STS values of 0.17 and 0.63 MPa were achieved for N_{TC} = 4 and 10, respectively (Figure 9(c)). Similarly, specimens treated with LAE produced STS values of 0.16 and 0.57 for N_{TC} = 4 and 10, respectively (Figure 9(d)). The increase in strength with increasing N_{TC} is due to an increased amount of precipitated calcium carbonate within the EICP-treated AI sand specimens, which induces bonding of soil particles (Ahenkorah *et al*., 2020a; Mahawish *et al*., 2019).

Improvement of strength with precipitated calcium carbonate

Figures 10(a) and 10(b) show a relationship between peak UCS (q_u) and STS (q_t) with M_{CaCO_3} for EICP-treated AI sand specimens. It is evident from this study that q_u and q_t increase exponentially with increasing M_{CaCO_3} irrespective of the type of enzyme used.

M_{CaCO_3} in the exponential trends in Figures 10(a) and 10(b) was replaced by values calculated from the terms on the right-hand side of Equation 1 and plotted in Figures 10(c) and 10(d). Almost identical trends were achieved in the two sets of figures, indicating a good prediction accuracy for Equation 1. This provides a unique relationship between q_u and $[E_g]/[S_0]$ for the soil treated as part of this study.

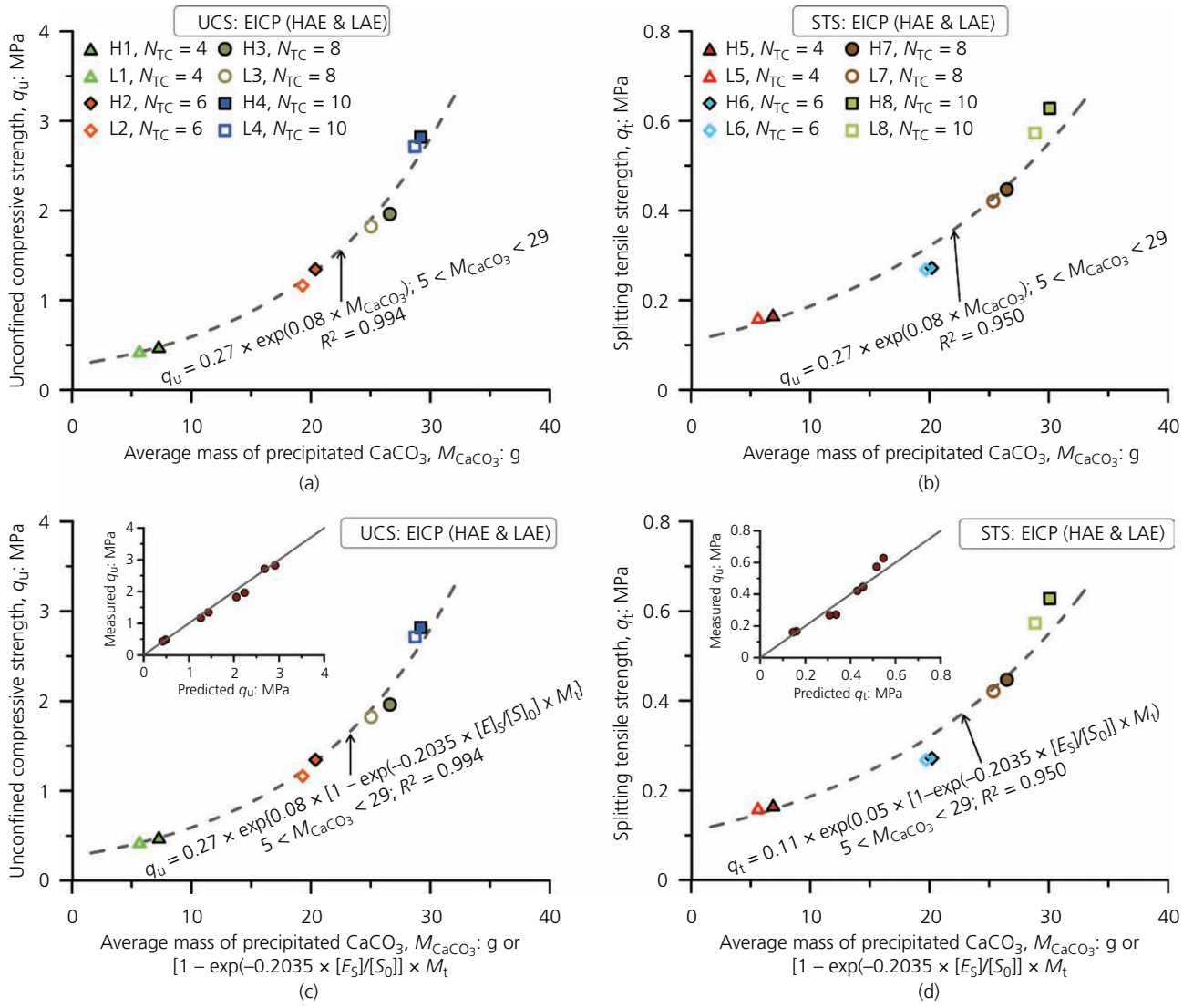

Figure 10. UCS plotted against (a) average M_{CaCO_3} and (c) average M_{CaCO_3} or Equation 1; STS plotted against (b) average M_{CaCO_3} and (d) average M_{CaCO_3} or Equation 1

Microstructural analysis of precipitated calcium carbonate

SEM and EDS analysis

Figures 11(a) and 11(b) show SEM images of precipitated calcium carbonate in the test tubes using LAE and HAE. The use of LAE led to precipitation of a significant quantity of anhedral calcite crystals, while the use of HAE resulted mainly in euhedral calcites. The difference in morphology was possibly due to the presence of impurities in the grade of urease enzyme used (Ahenkorah *et al*., 2020b).

Figures 12(a) and 12(b) show the SEM images of untreated clean sand while Figures 13(a)–13(d) show the images for different N_{TC} values for treated specimens using HAE. At $N_{TC} = 4$, a thin layer of precipitated calcium carbonate can be observed around the sand particles (see Figure 13(a)). With increasing N_{TC}, the thickness of the calcium carbonate layer increased and larger clusters of calcium carbonate deposits covering the sand grains were observed (see Figures 13(b)–13(d). A similar observation was made for SEM images of EICP-treated AI sand using LAE (Figures 14(a)–14(d)). By visual inspection, the majority of the calcium carbonate precipitation occurred at particle contacts with a very small proportion of calcium carbonate being deposited within the void spaces, as shown in Figures 13 and 14. The outcome of the SEM analysis was consistent with the earlier findings from the UCS and STS tests.

The EDS results for untreated AI sand at probe location 1 are shown in Figure 15(a), which indicates the presence of mainly silica (SiO_2) and oxygen (O) with small fractions of carbon and aluminium (Al). Figures 15(b) and 15(c) present the EDS results for probe locations 2 and 3, respectively, and these indicate the presence of mainly calcium (Ca), oxygen and carbon, implying the presence of calcium carbonate. However, since the morphology of the precipitated calcium carbonate cannot be confirmed through EDS, XRD analysis was performed.

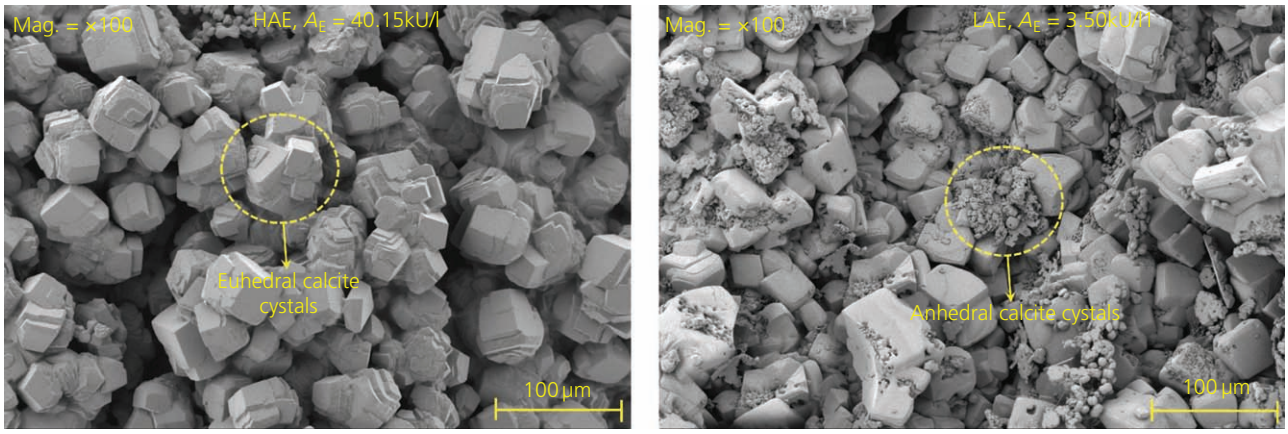

(a) (b)

Figure 11. Microstructures of test-tube-precipitated calcium carbonate: (a) SEM images for HAE; (b) SEM images for LAE

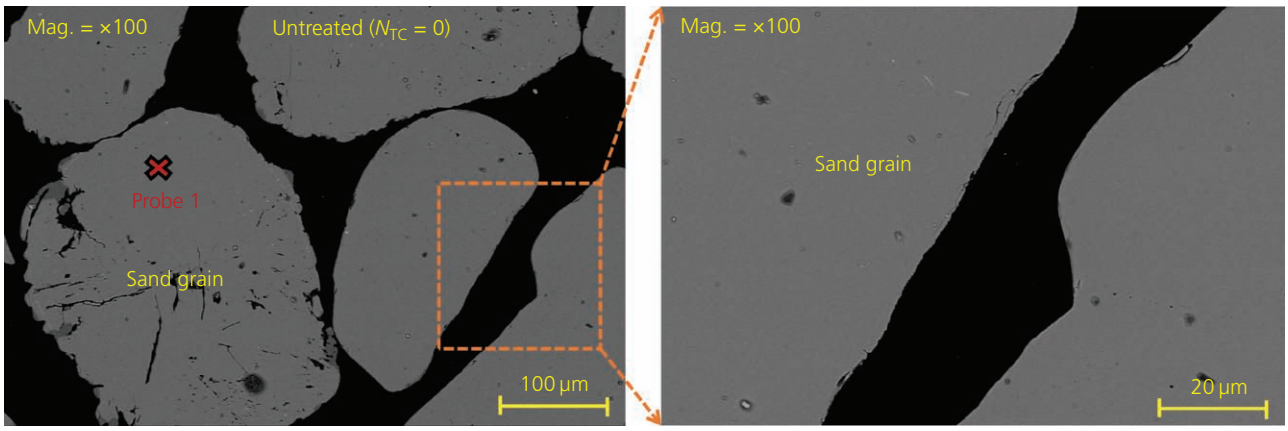

(a) (b)

Figure 12. SEM images of untreated AI sand: (a) ×200 magnification; (b) ×500 magnification

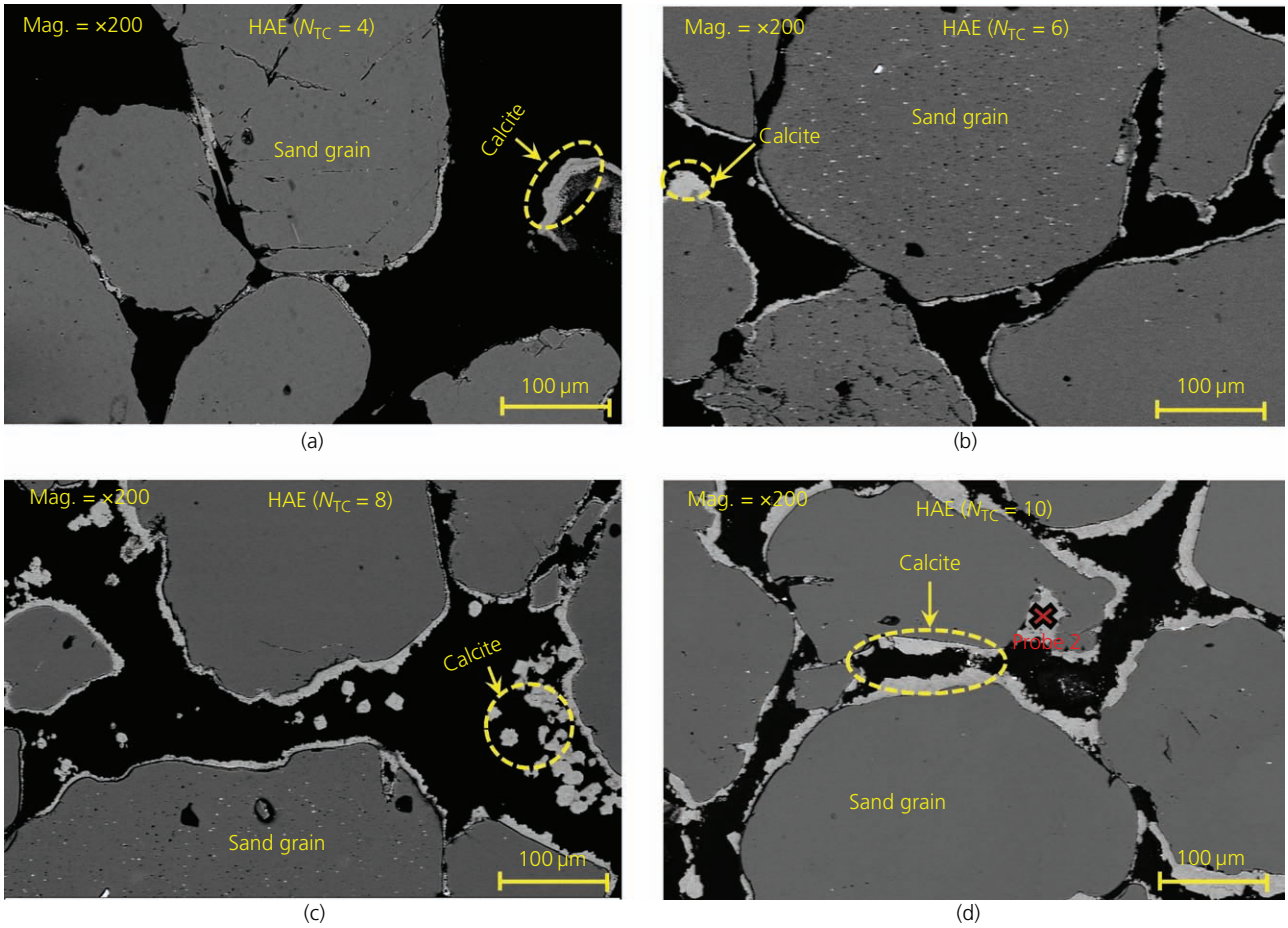

Figure 13. SEM images at ×200 magnification of EICP-treated sand specimens using HAE: (a) $4N_{TC}$; (b) $6N_{TC}$; (c) $8N_{TC}$; (d) $10N_{TC}$

XRD analysis

XRD tests were conducted to confirm the morphology of the calcium carbonate crystals observed in the SEM images, and the results are shown in Figures 16(a)–16(e). The XRD results of the precipitated calcium carbonate crystals from the test-tube experiments show high peaks for calcite crystals with minor traces of aragonite (for both LAE and HAE), as shown in Figures 16(a) and 16(b), respectively. Figure 16(c) shows the XRD analysis for the untreated clean AI sand where only traces of quartz can be found. Figures 16(d) and 16(e) show high peaks of quartz and calcite crystals with minor traces of aragonite for EICP-treated samples using HAE and LAE.

Discussion

The observations made from the test-tube experiments indicate that for each $[S_0]$, a particular amount of enzyme is needed to reach a particular value of PR and the quantity of enzyme needed is also dependent on its activity. This indicates that the substrate concentration, the enzyme concentration and the activity of the enzyme all influence PR. It should be noted that for the same substrate concentration, an increased quantity of enzyme or an increase in enzyme activity resulted in an increase in the value of $[E_s]/[S_0]$ as shown in Figure 6. An increase in $[E_s]/[S_0]$ beyond a threshold value of ~20 kU/mol did not affect the PR. The threshold value of $[E_s]/[S_0]$ to achieve PR = 100% was likely to be different if a different set of experimental parameters such as temperature or pH was chosen.

During urea hydrolysis, the substrate (urea) binds the active sites of the enzyme (Figure 17) and after formation of the product is released and becomes free to bind to a new substrate molecule (Robinson, 2015). At a much higher substrate concentration, the active sites of the enzyme become saturated, meaning all the enzymes are engaged in the catalytic reaction and the reaction proceeds at a maximum rate (for the enzyme concentration used). However, the rate of product formation may be significantly influenced by the presence of inhibitors (e.g. product inhibitors) or the degradation of urease enzyme over time (Ahenkorah *et al.*, 2021; Fidaleo and Lavecchia, 2003; Goličnik, 2013). Hence, the mass of product formed over time may be lower than the expected theoretical mass of product formation. One interesting observation that can be made from Figures 6(a) and 6(b) is that, despite using a range of different curing periods (1–14 days), the resulting PR still falls on the same line, and for a large proportion of the data

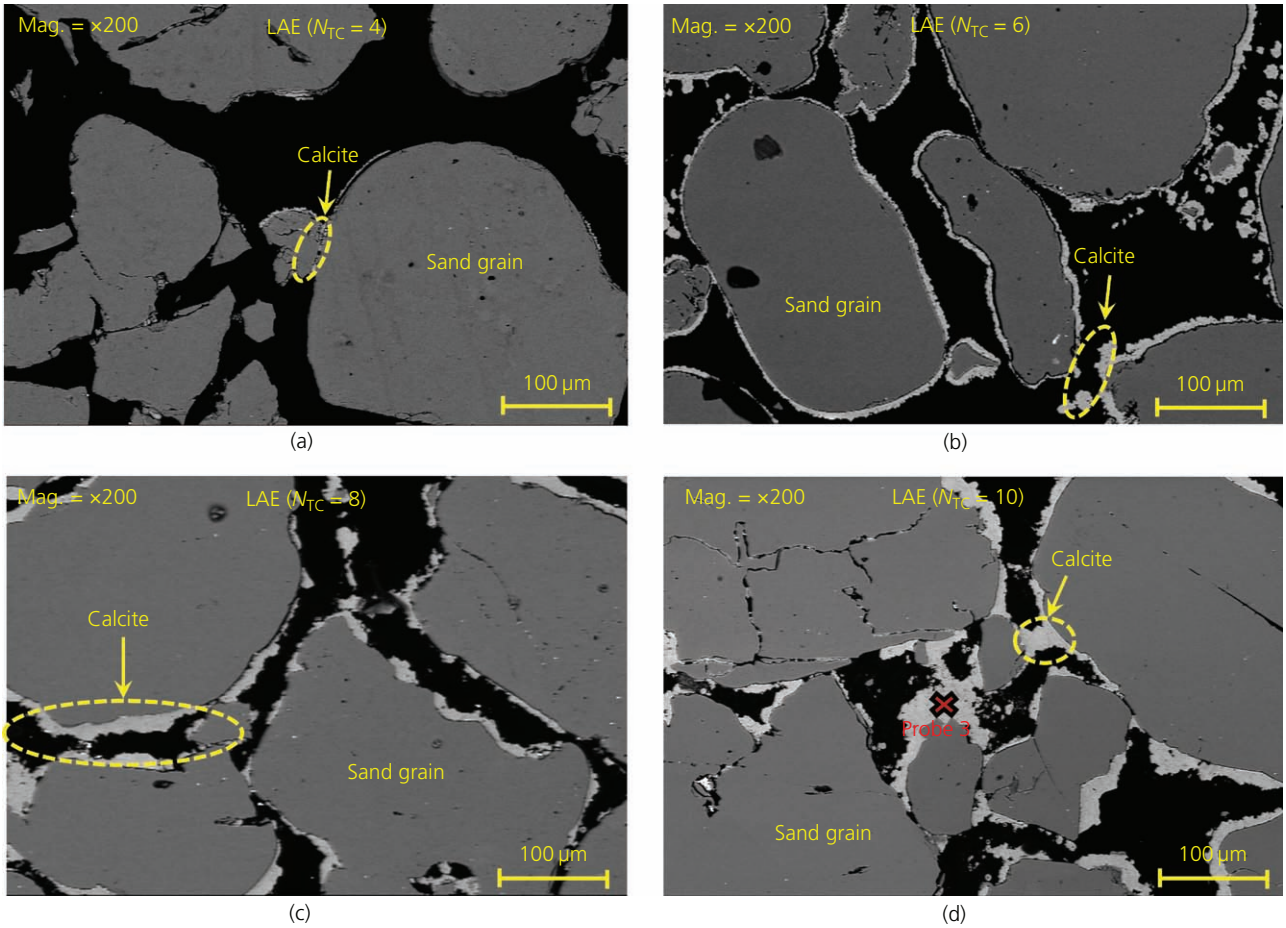

Figure 14. SEM images at ×200 magnification of EICP-treated sand specimens using LAE: (a) N_{TC} = 4; (b) N_{TC} = 6; (c) N_{TC} = 8; (e) N_{TC} = 10

points (PR<100%), the effect of curing time is not obvious apart from the small scatter observed in Figure 6(b). This indicates that the reaction rate is influenced by either product inhibition or degradation of enzymes and these effects are being indirectly captured by the ESF.

By using an optimum constituent concentration (i.e. $[E_s]/[S_0]$ = 20 kU/mol), it was found that the strengths obtained from both UCS and STS tests were not affected by the types of enzyme – that is, HAE and LAE. The average calcium carbonate PR for the EICP-treated sand specimens was around 97.5% for both HAE and LAE and was very similar to the PR values achieved in the test-tube tests.

The results of the SEM, EDS and XRD analysis indicated that the precipitated calcium carbonate in both the test tubes and soil treatments were mainly calcite crystals. Despite the differences in the morphology of the precipitated calcium carbonate in the test tubes using LAE and HAE, the overall strength behaviours (UCS and STS) for EICP-treated sand specimens were similar. This also suggests that using the optimum chemical constituent concentrations in this study produced similar macro- and micromechanical response irrespective of the type of enzyme used.

Conclusions

The influence of constituent concentration and enzyme activity on the effectiveness and microstructure of precipitated calcium carbonate during the EICP process was examined in this study. The major findings were as follows.

- The concentration of the substrate $[S_0]$ and enzyme $[E_0]$, as well as enzyme activity, affects the PR. The effect of enzyme concentration and activity on PR can be better explained using a normalisation of $[E_s] = [E_0]$ × activity. PR increased with increase in $[E_s]/[S_0]$ and reached 100% at a threshold $[E_s]/[S_0]$ value of approximately 20 kU/mol. Further increases in $[E_s]/[S_0]$ did not have any effect on PR.
- The PR was found to exhibit a non-linear correlation with $[E_s]/[S_0]$, and a first approximation exponential function was able to capture the relationship with reasonable accuracy. The function also captured the correlation between different

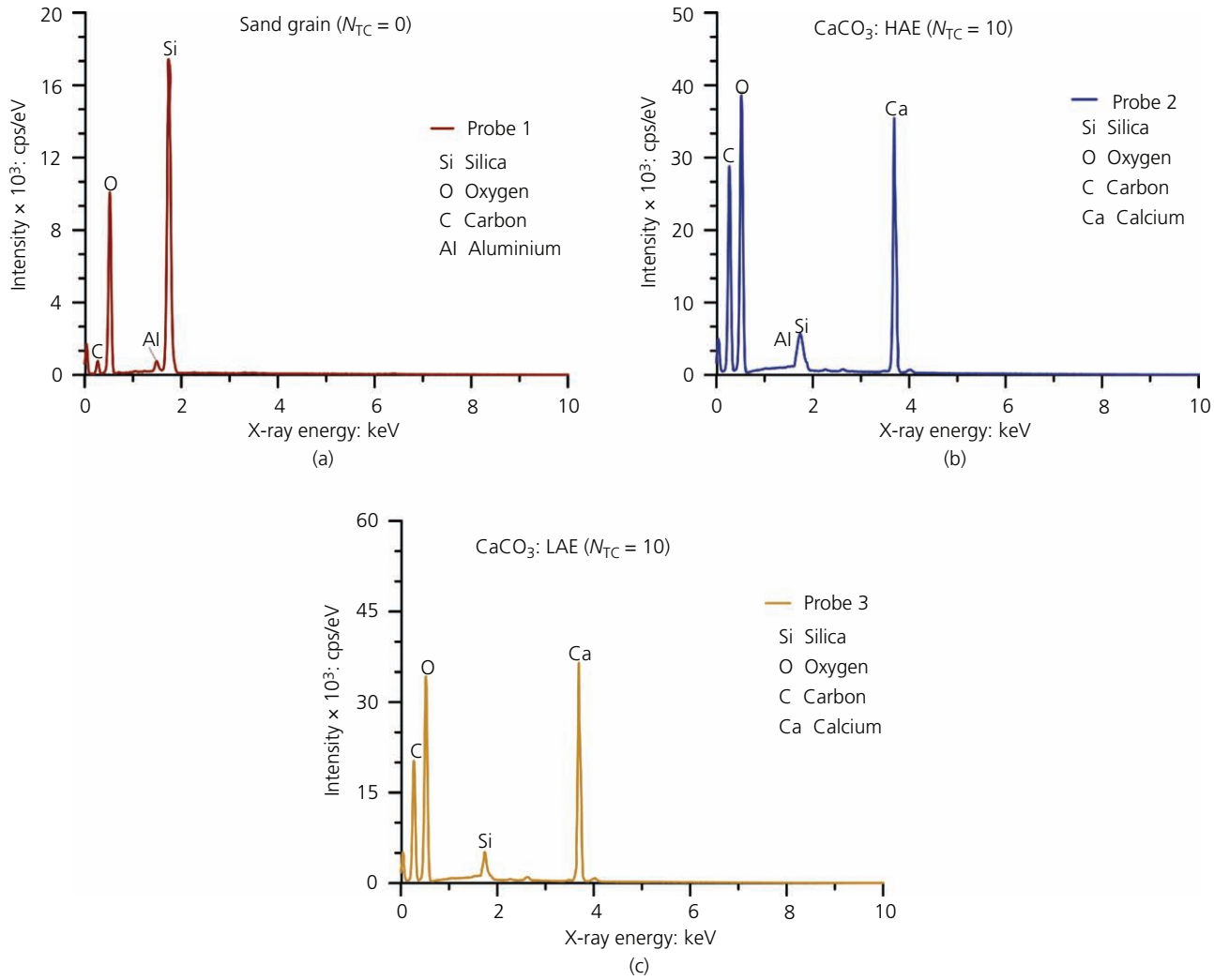

Figure 15. EDS results for selected regions (probes): (a) probe 1, sand grain; (b) probe 2, calcium carbonate precipitate for EICP-treated sand using HAE; (c) probe 3, calcium carbonate precipitate for treated sand using LAE

chemical constituents for more than 100 data points collected from the literature with reasonable accuracy.

- An optimum EICP solution consisting of $[E_s]/[S_0]$ = 20 kU/mol was used for soil treatment and produced a similar trend for UCS/STS and the mass of precipitated calcium carbonate. Functions were developed to capture the correlation between precipitated calcium carbonate mass and the strength (measured by UCS and STS) for a particular $[E_s]/[S_0]$ and gave a good prediction with reasonable accuracy.
- SEM images showed that the precipitates were calcite crystals with different morphologies and the differences were likely to be caused by the variation in the purity of the urease enzyme used. XRD analysis further indicated that the precipitated calcium carbonate in the test tubes and treated soils were mainly calcite crystals with traces of aragonite.

The findings of this study provide a clear understanding of how the concentration of the chemical constituents in EICP is influenced by the activity of the urease enzyme used. The optimum concentration threshold proposed may be significant for various engineering applications and will in effect increase the efficient use of chemical constituents (particularly urease enzyme), thereby reducing the amount of undesirable by-products for the EICP process.

Acknowledgements

The first author would like to acknowledge the Australian Government Research Training Program scholarship scheme for funding this research. This work was performed (in part) at the South Australian node of the Australian National Fabrication Facility under the National Collaborative Research Infrastructure Strategy.

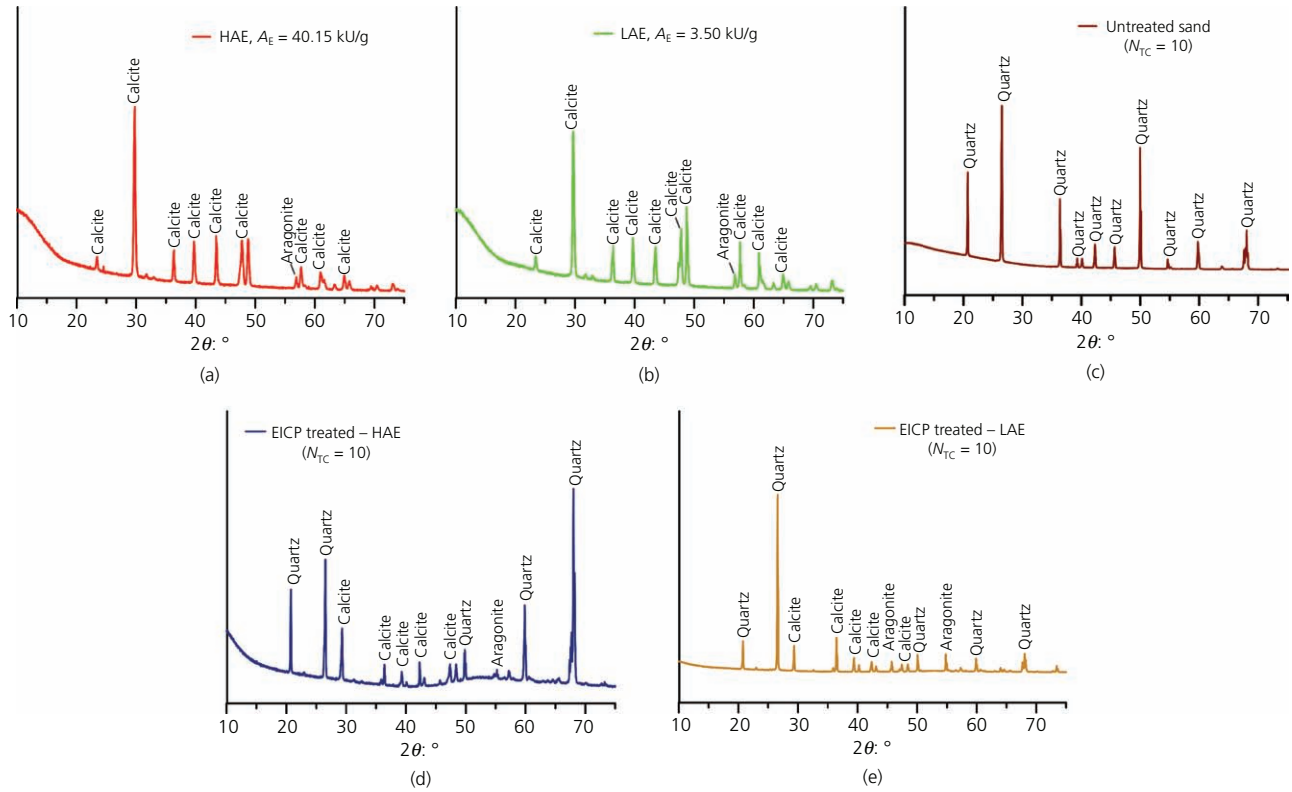

Figure 16. XRD spectra of (a) test-tube-precipitated calcium carbonate using HAE; (b) test-tube-precipitated calcium carbonate using LAE; (c) untreated AI sand; (d) EICP-treated sand using HAE; (e) EICP-treated sand using LAE

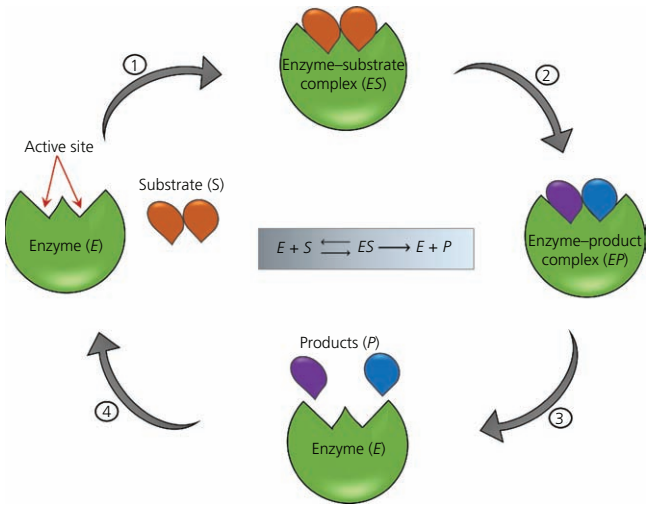

Figure 17. Schematic diagram of an enzyme–substrate reaction in EICP

REFERENCES

Ahenkorah I, Rahman MM, Karim MR and Teasdale PR (2020a) A comparison of mechanical responses for microbial and enzyme-induced cemented sand. *Géotechnique Letters* **10(4)**: 559–567, https://doi.org/10.1680/jgele.20.00061.

Ahenkorah I, Rahman MM, Karim MR and Teasdale PR (2020b) Optimization of enzyme induced carbonate precipitation (EICP) as a ground improvement technique. In *Geo-Congress 2020: Foundations, Soil Improvement, and Erosion* (Hambleton JP, Makhnenko R and Budge AS (eds)). American Society of Civil Engineers, Reston, VA, USA, pp. 552–561.

Ahenkorah I, Rahman MM, Karim MR, Beecham S and Saint C (2021) A review of enzyme induced carbonate precipitation (EICP): the role of enzyme kinetics. *Sustainable Chemistry* **2(1)**: 92–114, https://doi.org/10.3390/suschem2010007.

Almajed AA (2017) *Enzyme Induced Carbonate Precipitation (EICP) for Soil Improvement*. PhD thesis, Arizona State University, Tempe, AZ, USA.

Almajed A, Khodadadi Tirkolaei H and Kavazanjian E Jr (2018) Baseline investigation on enzyme-induced calcium carbonate precipitation. *Journal of Geotechnical and Geoenvironmental Engineering* **144(11)**: article 04018081, https://doi.org/10.1061/(ASCE)GT.1943-5606.0001973.

Almajed A, Tirkolaei HK, Kavazanjian E and Hamdan N (2019) Enzyme induced biocementated sand with high strength at low carbonate content. *Scientific Reports* **9(1)**: 1–7, https://doi.org/10.1038/s41598-018-38361-1.

ASTM (2016) D 2166: Standard test method for unconfined compressive strength of cohesive soil. ASTM International, West Conshohocken, PA, USA.

ASTM (2017a) D 2487: Standard practice for classification of soils for engineering purposes (Unified Soil Classification System). ASTM International, West Conshohocken, PA, USA.

ASTM (2017b) C 496: Standard test method for splitting tensile strength of cylindrical concrete specimens. ASTM International, West Conshohocken, PA, USA.

Carmona JP, Oliveira PJV and Lemos LJ (2016) Biostabilization of a sandy soil using enzymatic calcium carbonate precipitation. *Procedia Engineering* **143**: 1301–1308, https://doi.org/10.1016/j.proeng.2016.06.144.

Chen Y, Gao Y and Guo H (2021) Bio-improved hydraulic properties of sand treated by soybean urease induced carbonate precipitation and its application Part 2: Sand–geotextile capillary barrier effect. *Transportation Geotechnics* **27**: article 100484, https://doi.org/10.1016/j.trgeo.2020.100484.

Choi SG, Park SS, Wu S and Chu J (2017) Methods for calcium carbonate content measurement of biocemented soils. *Journal of Materials in Civil Engineering* **29(11)**: article 06017015, https://doi.org/10.1061/(ASCE)MT.1943-5533.0002064.

Cuccurullo A, Gallipoli D, Bruno A *et al.* (2019) Advances in the enzymatic stabilisation of soils. In *Proceedings of the 17th ECSMGE-2019: Geotechnical Engineering Foundation of the Future* (Sigursteinsson H, Erlingsson S and Bessason B (eds)). The Icelandic Geotechnical Society (IGS), Reykjavik, Iceland, pp. 1–8.

DeJong JT, Fritzges MB and Nusslein K (2006) Microbially induced cementation to control sand response to undrained shear. *Journal of Geotechnical and Geoenvironmental Engineering* **132(11)**: 1381–1392, https://doi.org/10.1061/(ASCE)1090-0241(2006)132:11(1381).

Dilrukshi R, Nakashima K and Kawasaki S (2018) Soil improvement using plant-derived urease-induced calcium carbonate precipitation. *Soils and Foundations* **58(4)**: 894–910, https://doi.org/10.1016/j.sandf.2018.04.003.

Fidaleo M and Lavecchia R (2003) Kinetic study of enzymatic urea hydrolysis in the pH range 4–9. *Chemical and Biochemical Engineering Quarterly* **17(4)**: 311–318.

Gao Y, He J, Tang X and Chu J (2019) Calcium carbonate precipitation catalyzed by soybean urease as an improvement method for fine-grained soil. *Soils and Foundations* **59(5)**: 1631–1637, https://doi.org/10.1016/j.sandf.2019.03.014.

Goličnik M (2013) The integrated Michaelis–Menten rate equation: déjà vu or vu jàdé? *Journal of Enzyme Inhibition and Medicinal Chemistry* **28(4)**: 879–893, https://doi.org/10.3109/14756366.2012.688039.

Hamdan NM (2015) *Applications of Enzyme Induced Carbonate Precipitation (EICP) for Soil Improvement*. PhD thesis, Arizona State University, Tempe, AZ, USA.

Hamdan N and Kavazanjian E (2016) Enzyme-induced carbonate mineral precipitation for fugitive dust control. *Géotechnique* **66(7)**: 546–555, https://doi.org/10.1680/jgeot.15.P.168.

Ismail MA, Joer HA, Sim WH and Randolph MF (2002) Effect of cement type on shear behavior of cemented calcareous soil. *Journal of Geotechnical and Geoenvironmental Engineering* **128(6)**: 520–529, https://doi.org/10.1061/(ASCE)1090-0241(2002)128:6(520).

Javadi N, Khodadadi H, Hamdan N and Kavazanjian E (2018) EICP treatment of soil by using urease enzyme extracted from watermelon seeds. In *IFCEE 2018: Innovations in Ground Improvement for Soils, Pavements, and Subgrades* (Stuedlein AW, Lemnitzer A and Suleiman MT (eds)). American Society of Civil Engineers, Reston, VA, USA, pp. 115–124.

Khodadadi TH, Javadi N, Krishnan V, Hamdan N and Kavazanjian EJ (2020) Crude urease extract for biocementation. *Journal of Materials in Civil Engineering* **32(12)**: article 04020374, https://doi.org/10.1061/(ASCE)MT.1943-5533.0003466.

Krajewska B (2009) Ureases I. Functional, catalytic and kinetic properties: a review. *Journal of Molecular Catalysis B: Enzymatic* **59(1)**: 9–21, https://doi.org/10.1016/j.molcatb.2009.01.003.

Krajewska B (2018) Urease-aided calcium carbonate mineralization for engineering applications: a review. *Journal of Advanced Research* **13**: 59–67, https://doi.org/10.1016/j.jare.2017.10.009.

Lee S and Kim J (2020) An experimental study on enzymatic-induced carbonate precipitation using yellow soybeans for soil stabilization. *KSCE Journal of Civil Engineering* **24(7)**: 2026–2037, https://doi.org/10.1007/s12205-020-1659-9.

Mahawish A, Bouazza A and Gates WP (2019) Unconfined compressive strength and visualization of the microstructure of coarse sand subjected to different biocementation levels. *Journal of Geotechnical and Geoenvironmental Engineering* **145(8)**: article 04019033, https://doi.org/10.1061/(ASCE)GT.1943-5606.0002066.

Martinez B, DeJong J, Ginn T *et al.* (2013) Experimental optimization of microbial-induced carbonate precipitation for soil improvement. *Journal of Geotechnical and Geoenvironmental Engineering* **139(4)**: 587–598, https://doi.org/10.1061/(ASCE)GT.1943-5606.0000787.

Mazzei L, Ciurli S and Zambelli B (2014) Hot biological catalysis: isothermal titration calorimetry to characterize enzymatic reactions. *Journal of Visualized Experiments* **86**: article e51487, https://doi.org/10.3791/51487.

Michaelis L and Menten ML (1913) Die Kinetik der Invertinwirkung. *Biochemische Zeitschrift* **49**: 333–369 (in German).

Mitchell JK and Santamarina JC (2005) Biological considerations in geotechnical engineering. *Journal of Geotechnical and Geoenvironmental Engineering* **131(10)**: 1222–1233, https://doi.org/10.1061/(ASCE)1090-0241(2005)131:10(1222).

Mortensen B and DeJong J (2011) Strength and stiffness of MICP treated sand subjected to various stress paths. In *Geo-Frontiers 2011: Advances in Geotechnical Engineering* (Han J and Alzamora DE (eds)). American Society of Civil Engineers, Reston, VA, USA, pp. 4012–4020.

Nafisi A, Safavizadeh S and Montoya BM (2019) Influence of microbe and enzyme-induced treatments on cemented sand shear response. *Journal of Geotechnical and Geoenvironmental Engineering* **145(9)**: article 06019008, https://doi.org/10.1061/(ASCE)GT.1943-5606.0002111.

Nam IH, Chon CM, Jung KY *et al.* (2015) Calcite precipitation by ureolytic plant (*Canavalia ensiformis*) extracts as effective biomaterials. *KSCE Journal of Civil Engineering* **19(6)**: 1620–1625, https://doi.org/10.1007/s12205-014-0558-3.

Nassar MK, Gurung D, Bastani M *et al.* (2018) Large-scale experiments in microbially induced calcite precipitation (MICP): reactive transport model development and prediction. *Water Resources Research* **54(1)**: 480–500, https://doi.org/10.1002/2017WR021488.

Neupane D, Yasuhara H, Kinoshita N and Unno T (2013) Applicability of enzymatic calcium carbonate precipitation as a soil-strengthening technique. *Journal of Geotechnical and Geoenvironmental Engineering* **139(12)**: 2201–2211, https://doi.org/10.1061/(ASCE)GT.1943-5606.0000959.

Neupane D, Yasuhara H, Kinoshita N and Ando Y (2015) Distribution of mineralized carbonate and its quantification method in enzyme mediated calcite precipitation technique. *Soils and Foundations* **55(2)**: 447–457, https://doi.org/10.1016/j.sandf.2015.02.018.

Pratama G, Yasuhara H, Kinoshita N and Putra H (2021) Application of soybean powder as urease enzyme replacement on EICP method for soil improvement technique. *IOP Conference Series: Earth and Environmental Science* **622**: 012035, https://doi.org/10.1088/1755-1315/622/1/012035.

Putra H, Yasuhara H, Kinoshita N and Neupane D (2015) Optimization of calcite precipitation as a soil improvement technique. *Proceedings of the 2nd Makassar International Conference on Civil Engineering, Makassar, Indonesia*, pp. 11–12.

Putra H, Yasuhara H and Kinoshita N (2017a) Applicability of natural zeolite for NH-forms removal in enzyme-mediated calcite precipitation technique. *Geosciences* **7(3)**: article 61, https://doi.org/10.3390/geosciences7030061.

Putra H, Yasuhara H and Kinoshita N (2017b) Optimum condition for the application of enzyme-mediated calcite precipitation technique as soil improvement technique. *International Journal on Advanced Science, Engineering and Information Technology* **7(6)**: 2145–2151, https://doi.org/10.18517/ijaseit.7.6.3425.

Rahman MM, Hora NR, Ahenkorah I *et al.* (2020) State-of-the-art review of microbial induced calcite precipitation and its sustainability in engineering applications. *Sustainability* **12(15)**: article 6281, https://doi.org/10.3390/su12156281.

Robinson PK (2015) Enzymes: principles and biotechnological applications. *Essays in Biochemistry* **59**: 1–41, https://doi.org/10.1042/bse0590001.

Song JY, Sim Y, Jang J, Hong WT and Yun TS (2020) Near-surface soil stabilization by enzyme-induced carbonate precipitation for fugitive dust suppression. *Acta Geotechnica* **15(7)**: 1967–1980, https://doi.org/10.1007/s11440-019-00881-z.

Wen KJ, Li Y, Amini F and Li L (2020) Impact of bacteria and urease concentration on precipitation kinetics and crystal morphology of calcium carbonate. *Acta Geotechnica* **15(1)**: 17–27, https://doi.org/10.1007/s11440-019-00899-3.

Whiffin VS (2004) *Microbial CaCO 3: Precipitation for the Production of Biocement*. PhD thesis, Murdoch University, Perth, Australia.

Xiao Y, He X, Evans TM, Stuedlein AW and Liu H (2019) Unconfined compressive and splitting tensile strength of basalt fiber–reinforced biocemented sand. *Journal of Geotechnical and Geoenvironmental Engineering* **145(9)**: article 04019048, https://doi.org/10.1061/(ASCE)GT.1943-5606.0002108.

Yasuhara H, Neupane D, Hayashi K and Okamura M (2012) Experiments and predictions of physical properties of sand cemented by enzymatically-induced carbonate precipitation. *Soils and Foundations* **52(3)**: 539–549, https://doi.org/10.1016/j.sandf.2012.05.011.

Yuan H, Ren G, Liu K, Zheng W and Zhao Z (2020) Experimental study of EICP combined with organic materials for silt improvement in the Yellow River flood area. *Applied Sciences* **10(21)**: article 7678, https://doi.org/10.3390/app10217678.

Zimmer M (2000) Molecular mechanics evaluation of the proposed mechanisms for the degradation of urea by urease. *Journal of Biomolecular Structure and Dynamics* **17(5)**: 787–797, https://doi.org/10.1080/07391102.2000.10506568.

How can you contribute?

To discuss this paper, please submit up to 500 words to the editor at journals@ice.org.uk. Your contribution will be forwarded to the author(s) for a reply and, if considered appropriate by the editorial board, it will be published as a discussion in a future issue of the journal.